

Constitutive Relation by Regression Reveals Scaling Law for Hydrodynamic Transport Coefficients

Candi Zheng,^{1,2,*} Yang Wang,^{2,†} and Shiyi Chen^{1,‡}

¹*Department of Mechanics and Aerospace Engineering,*

Southern University of Science and Technology, Xueyuan Rd 1088, Shenzhen, China

²*Department of Mathematics, Hong Kong University of Science and Technology, Clear Water Bay, Hong Kong SAR, China*

(Dated: November 23, 2021)

Finding extended hydrodynamics equations valid from the dense gas region to the rarefied gas region remains a great challenge. The key to success is to obtain accurate constitutive relations for stress and heat flux. Recent data-driven models offer a new phenomenological approach to learning constitutive relations from data. Such models enable complex constitutive relations that extend Newton's law of viscosity and Fourier's law of heat conduction, by regression on higher derivatives. However, choices of derivatives in these models are ad-hoc without a clear physical explanation. We investigated data-driven models theoretically on a linear system. We argue that these models are equivalent to non-linear length scale scaling laws of transport coefficients. The equivalence to scaling laws justified the physical plausibility and revealed the limitation of data-driven models. Our argument also points out modeling the scaling law explicitly could avoid practical difficulties in data-driven models like derivative estimation and variable selection on noisy data. We further proposed a constitutive relation model based on scaling law and tested it on the calculation of Rayleigh scattering spectra. The result shows data-driven model has a clear advantage over the Chapman-Enskog expansion and moment methods for the first time.

Introduction Rarefied gas dynamics are widely encountered in aerospace engineering practices such as re-entry [1], space station maintenance [2], and Lidar wind measurement [3]. Rarefied gas flow simulation is known to be difficult due to the non-negligible dynamics at the mesoscopic scale. Simulation resolving these scales is computationally expensive for continuous and transitional flows, such as the Direct Simulation Monte Carlo (DSMC) [4] method. Instead, extended hydrodynamics equations at coarse-grained macroscopic scale are efficient substitutes to reduce the computational cost. What lies within the heart of extended hydrodynamics is constitutive relations. Constitutive relations summarize mesoscopic scale dynamics as macroscopic phenomena, such as viscosity and heat conduction. Traditionally they are modeled by perturbation or expansion around the equilibrium of dense gas as in Hilbert-Chapman-Enskog theory [5–7], Grad moment method [8] and its extensions[9]. However difficulties exist including stability issue[10], unphysical solutions[11] and limited applicable Knudsen numbers range[9].

Data-Driven models offer a new phenomenological approach to obtain constitutive relations from data. It is expected to expand the applicable range of extended hydrodynamics equations[12]. There have been attempts to learn constitutive relations from mesoscopic results [13] or to find proper moment equations [12]. Data-Driven models are also used in related areas such as learning the unknown governing of physical systems[14–17], simulating physical dynamics [18–20] and solving the Boltzmann

equation [21]. These attempts have proven the concept of data-driven modeling. However, the advantage over traditional models like Chapman-Enskog and Grad moment method hasn't been established yet. Limitations for data-driven models include derivative estimation [22], determining input quantities (variable selection)[16], and how to model across a range of Knudsen numbers. Besides, the rather ad-hoc linear or neural network regression in data-driven models lack a clear physical explanation.

In this letter, we investigate data-driven models on linear systems. We focus on the conservation equations for mass, momentum, and energy. We analyze linear constitutive relation models that extend Newton's law of viscosity and Fourier's law of heat conduction, by regression on high-order derivatives of density, velocity, and temperature. We argue that these models, although linear, are equivalent to non-linear length scale scaling laws of viscosity and heat conduction coefficients. These length scale scaling laws describe the change of viscosity and heat conduction coefficients, as we concern dynamics at different length scales described by Knudsen numbers. The equivalence to scaling laws justified the physical plausibility of data-driven models. It also reveals two facts: 1. High-order derivatives in constitutive relations help to model more flexible scaling laws. 2. Memory and long-range effects that could not be described by scaling laws of transport coefficients require more equations, rather than high-order derivatives.

Based on our argument, we suggest modeling scaling laws explicitly in data-driven models. In doing so, we could involve high-order derivatives implicitly in constitutive relations without calculating them. It helps to avoid practical difficulties in data-driven models like derivative estimation and variable selection. We further

* zhengcd@mail.sustech.edu.cn, czhengac@connect.ust.hk

† yangwang@ust.hk

‡ chensy@sustech.edu.cn, corresponding author

modeled the constitutive relation based on our suggestion. In the numerical experiment, we apply our model to calculate the Rayleigh scattering spectra. Our data-driven model, to our knowledge, significantly outperform the Chapman-Enskog expansion and Grad moment methods for the first time.

Methods We consider the linearized extended hydrodynamics for one-dimensional rarefied idea gas. The dynamics of gas is governed by the hydrodynamics equations. They form a 1D linear system of the non-dimensionalized density ρ , velocity v , and temperature T , corresponding to conservation laws for mass, momentum, and energy respectively. However, the hydrodynamics equations are not closed with two extra unknown terms: the stress σ and the heat flux q that encodes the mesoscopic dynamics. To close the equations, constitutive relations that model the stress and the heat flux with known quantities are necessary.

Constitutive relations such as Newton's law of viscosity $\sigma = -\frac{4}{3}\mu_0\partial_x v$ and Fourier's law of heat conduction $q = -\kappa_0\partial_x T$ are not capable to describe rarefied gas effects [23], in which μ_0 is the viscosity coefficient and κ_0 is the heat conduction coefficient. To extend the capability of constitutive relation, we could incorporate high-order derivatives of density, velocity, and temperature [24]. For linear system we consider the data-driven constitutive relation model of non-dimensional stress σ and heat flux q as in (1), where x is the non-dimensional spatial coordinate, $a_n, b_n, c_n, d_n, e_n, f_n$ are unknown *regression coefficients* to be learned from data.

$$\begin{aligned}\sigma &= -\sum_{n=1}^{\infty} \left(a_n \frac{\partial^n v}{\partial x^n} + c_n \frac{\partial^n \rho}{\partial x^n} + e_n \frac{\partial^n T}{\partial x^n} \right) \\ q &= -\sum_{n=1}^{\infty} \left(b_n \frac{\partial^n T}{\partial x^n} + d_n \frac{\partial^n \rho}{\partial x^n} + f_n \frac{\partial^n v}{\partial x^n} \right).\end{aligned}\quad (1)$$

However, constitutive relation (1) does not guarantee the stability of hydrodynamic equations. To ensure stability, the entropy of the system must be non-decreasing. This constraint on entropy leads to the equivalence between constitutive relation model (1) and scaling laws of viscosity and heat conduction coefficients. The outline of the argument is as follows: Firstly, we claim that the constitution relation for stress σ consists of only velocity derivatives, while the constitution relation for heat flux q consists of only temperature derivatives. This is because the stress and velocity, same as heat flux and temperature, must be correlated to produce non-increasing entropy as

$$\dot{s} = -\frac{q}{T^2}\partial_x T - \frac{\sigma}{T}\partial_x v, \quad (2)$$

where \dot{s} is the entropy change rate per mass [25]. The only possibility is stress depends on velocity only, the same as heat flux depending on temperature, since density, velocity, and temperature are statistically independent [26]. Secondly, even-order derivatives vanish in constitution relation (1) because the entropy change rate (2)

must be real and non-negative in the Fourier space. Finally, collecting the summation in (1) over the infinite terms leads to the production form in the Fourier space,

$$\begin{aligned}\sigma(k) &= -ik \frac{4}{3} \frac{\mu(k)}{\mu_0} \tilde{v}_k; \quad \mu(k) \geq 0 \\ q(k) &= -ik \frac{\kappa(k)}{\kappa_0} \tilde{T}_k; \quad \kappa(k) \geq 0,\end{aligned}\quad (3)$$

where μ_0 is the viscosity coefficient, κ_0 is the heat conduction coefficient, k is the non-dimensional wavenumber for each Fourier mode, \tilde{v}_k, \tilde{T}_k are corresponding spatial Fourier modes of v, T . The functions $\mu(k), \kappa(k)$ are even functions satisfy the natural constraints $\mu_0 = \lim_{k \rightarrow 0} \mu(k)$ and $\kappa_0 = \lim_{k \rightarrow 0} \kappa(k)$. They describes the length scaling law for viscosity and heat conduction coefficient, as we will discuss later. In short, the constitutive relation (1) reduces to the production form (3) in the Fourier space to ensure the stability of the hydrodynamic system.

The functions $\mu(k), \kappa(k)$ are the length scaling laws of viscosity and heat conduction coefficients. They describe the relative change of viscosity and heat conduction coefficients w.r.t length scale changes of the system. This is because k is closely related to the *Knudsen number* $\text{Kn} = l/L$ that characterize the length scale of a rarefied gas system, in which l is the mean free path of gas molecules and L is the representative length scale of the system. Particularly, we have

$$k = \pm \text{Kn} \quad (4)$$

if we choose the representative length scale L to be the wavelength of Fourier mode with non-dimensional wavenumber k . The scaling laws could be measured experimentally [27]. However, we can not use experimental results directly because the definition of the Knudsen number is not unified, but varies according to the experiment setting. Alternatively, data like fluctuation spectra contain viscosity information [28] and could be further used to learn scaling laws.

Constitutive relations using scaling laws (3) converge more uniformly for various Knudsen numbers than the original regression (1). Derivatives in (1) only contribute polynomials of k to the scaling laws $\mu(k), \kappa(k)$, which converge only when k is small. Instead, $\mu(k), \kappa(k)$ in (3) could be implemented using neural networks. These neural networks will be trained on data at various Knudsen hence converging uniformly. Moreover, this formulation is highly robust against noisy data because it avoids using estimated derivatives. In addition, This formulation avoided the variable selection problem for infinite *regression coefficients*. The viability of our argument could be confirmed if this model performs well on a benchmark test.

We test our argument by calculating the Rayleigh scattering spectra. The *Rayleigh scattering* describes the refraction of electromagnetic waves (EM waves) passing through media with stochastic density fluctuation

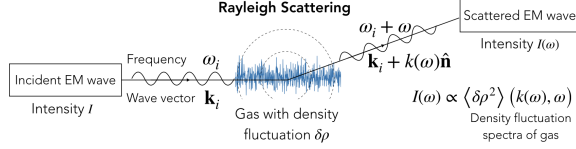


FIG. 1. Rayleigh scattering of electromagnetic(EM) waves with wave vector \mathbf{k}_i and frequency ω_i through gas with density fluctuation $\delta\rho$. $\hat{\mathbf{n}}$ is a unit vector. The intensity $I(\omega)$ of scattered EM wave with frequency shift ω is the Rayleigh scattering spectra. The Rayleigh scattering spectra are proportional to and determined by the density fluctuation spectra $\langle\delta\rho^2\rangle$. Therefore to compute the Rayleigh scattering spectra, we need only to compute the density fluctuation spectra of gas.

[29, 30]. Such fluctuation usually appears as density fluctuation waves and happens spontaneously with the thermal motion of gas molecules. The *Rayleigh scattering spectra* are defined as the intensities $I(\omega)$ of scattered EM waves after the Rayleigh scattering with frequency shifts ω , as shown in Fig 1. They are proportional to the density fluctuation spectra of gas [31, 32]

$$I(\omega) \propto \langle\delta\rho^2\rangle(k(\omega), \omega), \quad (5)$$

where k is the wavenumber change of the scattered EM wave and $\langle\delta\rho^2\rangle$ is the *density fluctuation spectra*, which describes the intensity of density fluctuation waves at each wavenumber k and frequency ω . Consequently to calculate the Rayleigh scattering spectra all we need is to compute the density fluctuation spectra of the gas media.

The density fluctuation spectra $\langle\delta\rho^2\rangle(k, \omega)$ could be calculated from macroscopic governing equations using constitutive relation (3). We model functions μ, κ using neural networks. We constraint the neural network value and derivative at $k = 0$ to guarantee consistency with the Navier-Stokes equation. In addition, we couple κ and μ together

$$\kappa(k) = \frac{5k_B}{2m} \frac{\mu(k)}{\text{Pr}}, \quad \text{Pr} = \frac{2}{3} \quad (6)$$

to constraint the Prandtl number Pr to the Chapman-Enskog result $\text{Pr} = \frac{2}{3}$. While for training our model this coupling isn't necessary, we have chosen to do so because it makes sense physically, and it does accelerate the learning process without undermining the accuracy. To satisfy all these constraints, we design the following non-dimensional constrained neural network $M(\text{Kn}) = \frac{4}{3} \frac{\mu(\text{Kn})}{\mu_0}$ with the architecture

$$M(\text{Kn}) = \frac{4}{3} (1 + \mathbf{W}_2 \cdot \text{Tanh}(\mathbf{W}_1 \cdot \mathcal{H}(20\text{Kn}))) \quad (7)$$

$$\mathcal{H}(x) = \frac{1}{2}x^2, x < 1; \quad |x| - \frac{1}{2}, x \geq 1,$$

in which Kn satisfy (4), $\mathbf{W}_1, \mathbf{W}_2$ are the one-dimension weights vector of the neural network, with the activation

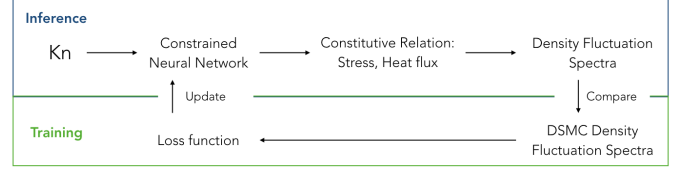


FIG. 2. The flow chart of our model to calculate the density fluctuation spectra.

function Tanh acting element-wise on the vector input. The function $M(\text{Kn})$ is even and satisfies $M'(0) = 0$. It guarantee the consistency with the NS equation.

The next step will be learning the weights vector $\mathbf{W}_1, \mathbf{W}_2$ in the neural network from data. This requires a loss function as the learning target. In our case, the loss function compares the difference between the observed spectra $\langle\delta\rho^2\rangle_{\text{dsmc}}$ and predicted spectra $\langle\delta\rho^2\rangle$. The former are results from the DSMC method, while the latter are the predictions of the governing equation. We define the loss function for any input weight vector $\mathbf{W} = \mathbf{W}_1, \mathbf{W}_2$ as

$$L(\mathbf{W}) = \mathbb{E}_{\text{Kn} \sim U} \mathbb{E}_{\omega \sim p(\omega|\text{Kn})} |\langle\delta\rho^2\rangle_{\text{dsmc}}(\text{Kn}, \omega) - \langle\delta\rho^2\rangle(\text{Kn}, \omega; \mathbf{W})|^2, \quad (8)$$

in which the predicted spectra $\langle\rho^2\rangle$ is a function on the weights vectors \mathbf{W} because it depends on the neural network $M(\text{Kn})$. The symbol $\mathbb{E}_{\text{Kn} \sim U}$ represents taking the expectation numerically by sampling Kn from a uniform distribution U . Meanwhile, $\mathbb{E}_{\omega \sim p(\omega|\text{Kn})}$ represents taking the expectation by sampling ω from a conditional distribution $p(\omega|k)$, which is proportional to the amplitude of the DSMC spectra. Sampling ω in this way makes the sample point lies more in the peak region. After defining the loss function, we use the ADAM [33] optimizer to minimize the loss function and determine the weights vector.

In total, the numerical experimental setting could be divided into two processes: inference and training. The inference process calculates the density fluctuation spectra using the governing equations with the constitutive relations (3). The constitutive relations contain neural networks M, K defined in (6) and (7) with weights to be determined. The training process determines the weights of neural networks by minimizing the loss function (8). The flow chart Fig 2 summarizes the entire procedure.

Results We compare the density fluctuation spectra calculated by our model with the results of the NS equation and the Grad 13 method. For various Knudsen numbers, spectra $\langle\delta\rho^2\rangle(\tilde{\omega})$ are shown in Fig 3 as function of the non-dimensionalized frequency $\tilde{\omega}$. At a small Knudsen number, all models give consistent spectra. However, At large Knudsen number, our model result matches nicely with the DSMC result, while the shape and amplitude of the NS equation and Grad 13 moments method deviate. Therefore, compared with the NS equation and

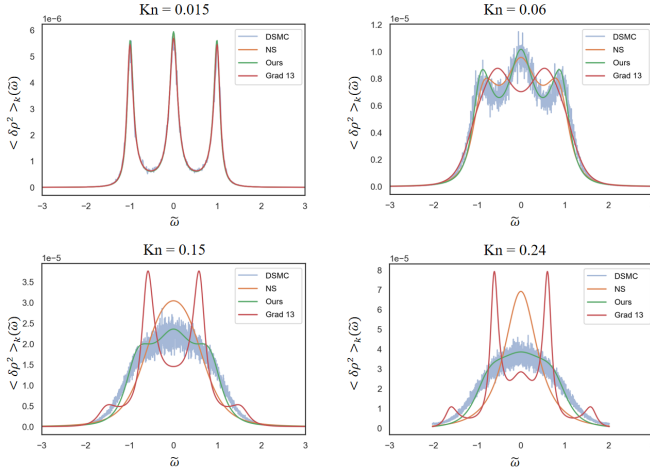


FIG. 3. Comparison between spectra calculated using DSMC, the NS equation, the Grad 13 method, and our model for various Knudsen numbers. At a small Knudsen number, The spectra consist of three peaks corresponds to entropy fluctuation and pressure fluctuation. As the Knudsen number increase, these peaks disappear gradually and blur into a bell shape. The result showed that our model calculated spectra match the DSMC result much better than the NS equation and Grad 13 method, especially in the high Knudsen number region.

the Grad 13 method, our model gives the most accurate spectra which are close to the DSMC result in both shape and amplitude.

We test our model performance on predicting the velocity fluctuation spectra to show its generalization ability. The generalization ability ensures that, rather than force to reproduce the DSMC spectra, our model learns the rarefied dynamic physics. To prove it did learn physics, we let our model predicts the velocity fluctuation spectra which our model has never seen as data. The result is shown in Fig 4(a). our model gives the correct shape that is much better than the NS equation. Consequently, our model has the generalization ability to predict spectra of other quantities, hence did learn the rarefied dynamic physics.

The rarefied dynamic physics learned from data is encoded in neural network M . We plot the neural network M in Fig 4(b) as the function $M(\text{Kn})$ multiplied by Kn . The corresponding function for the NS equation is also plotted because the NS equation also lies in our model framework. At the origin, these two plots are tangent, indicating our model is consistent with the NS equation. As the Knudsen number increase, the plot for our model bends downward. This downward bend means that viscosity decrease as the Knudsen number increase.

Discussion We have given the data-driven model a clear physical explanation, by pointing out the equivalence between constitutive relation by linear regression and scaling law for transport coefficients. High-order derivatives give constitutive relations the power to model

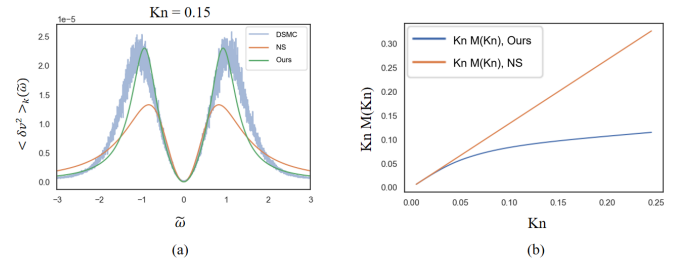


FIG. 4. (a) The test comparison between our model and NS equation predicted velocity fluctuation spectra with DSMC results at Knudsen number $\text{Kn} = 0.15$. Though our model has never trained on the velocity fluctuation spectra, it still outperforms the NS equation. Therefore our model has generalization ability, hence did learn the rarefied dynamic physics. (b) The function $M(\text{Kn})$ multiplied by Kn inferred from DSMC data by our model, compared with the corresponding function for the NS equation. They are consistent when the Knudsen number is small.

more flexible and accurate scaling laws. The reason is additional terms of high-order derivatives in (1) contribute additional high order polynomials to scaling functions in (3). However, limited by the Markov nature of transport coefficients, scaling laws will not help for phenomena with memory or long-range effects like upstream effect to downstream in shock wave structure. Such effects require additional equations and can not be described merely by transport coefficients. Succinctly, our explanation unfolds the power and limit of data-driven constitutive relation by regression on high-order derivatives.

Our argument not only gives a physical explanation but also helps to avoid practical problems in regression. Instead of regression on derivatives, we suggest directly model the scaling functions. It helps to avoid two major problems in regression on derivatives: derivative estimation and variable selection. Derivative estimation encounter stability and accuracy issue for high-order derivatives. Directly model the scaling functions on scaling variables avoids this without undermining its flexibility. Variable selection for infinite many regression coefficients in (1) is difficult even if sparsity methods are involved. Directly model the scaling functions could use a better basis with finite regression coefficients. In total, our argument suggests a better formulation for data-driven modeling.

Our model showed that the data-driven approach has the advantage over perturbation and moment expansion methods, corresponding to the NS equation and the Grad 13 method accordingly. Limited by their slow convergence rate at large Knudsen number, higher-order perturbation or moment expansion benefit little for more accurate spectra at large Knudsen numbers[34]. Instead, our model learns the rarefied gas dynamics from data points equally, hence converge uniformly for various Knudsen numbers. As we have shown in the result section, our model outperforms the NS equation and the Grad 13

method using only three conservation laws. Therefore the data-driven approach has demonstrated a clear advantage in handling rarefied gas dynamics.

Further investigation on constraints of data-driven models is necessary. We believe data-driven models directly model stress and heat flux is unsuitable for strong non-Maxwellian dynamics, such as shock waves fronts. Counter-intuitively, the reason for the unsuitability is a lack of constraints rather than flexibility. Unlike Maxwell distribution, strong non-Maxwellian dynamics tend to have distribution with irregular shapes. Such irregularity will correlate stress and heat flux. Hence proper constraints on stress between heat flux are required. Data-driven models with constrained constitutive relations maybe a future direction for strong non-Maxwellian dynamics.

In summary, we argued that the data-driven regression models for constitutive relation are equivalent to length scaling laws of transport coefficients. Our argument not only provides a theoretical justification for data-driven

models but also helps to avoid practical problems. We further modeled constitutive relation based on our argumentation. On calculating the Rayleigh scattering spectra, our model significantly outperforms the Chapman-Enskog expansion and Grad moment methods. Our argumentation also reveals the limitation of data-driven constitutive relation. It is not suitable for phenomena with memory or long-range effects unless accompanied by additional equations. In addition, further constraints are necessary for it to accommodate strong non-equilibrium dynamics.

ACKNOWLEDGMENTS

We wish to acknowledge Professor Lei Wu (Southern University of Science and Technology) in offering suggestions on Rayleigh scattering modeling. We thank Ms Yuan Lan (Hong Kong University of Science and Technology) for comments on the manuscript.

-
- [1] E. P. Muntz, Rarefied Gas Dynamics, Annual Review of Fluid Mechanics 10.1146/annurev.fl.21.010189.002131 (1989).
 - [2] Spacecraft charging: A review, in *Space Systems and Their Interactions with Earth's Space Environment*, pp. 167–226.
 - [3] G. Fiocco and J. DeWolf, Frequency spectrum of laser echoes from atmospheric constituents and determination of the aerosol content of air, Journal of Atmospheric Sciences **25**, 488 (1968).
 - [4] G. A. Bird, Molecular gas dynamics and the direct simulation of gas flows - 2nd edition (1994).
 - [5] D. Hilbert, Begründung der kinetischen Gastheorie, Mathematische Annalen 10.1007/BF01456676 (1912).
 - [6] VI. On the law of distribution of molecular velocities, and on the theory of viscosity and thermal conduction, in a non-uniform simple monatomic gas, Philosophical Transactions of the Royal Society of London. Series A, Containing Papers of a Mathematical or Physical Character 10.1098/rsta.1916.0006 (1916).
 - [7] D. Enskog, Kinetische theorie der vorgänge in mässig verdünnten gasen. i. allgemeiner teil, Uppsala: Almqvist & Wiksells Boktryckeri (1917).
 - [8] H. Grad, On the kinetic theory of rarefied gases, Communications on Pure and Applied Mathematics **2**, 331 (1949).
 - [9] H. Struchtrup and P. Taheri, Macroscopic transport models for rarefied gas flows: A brief review, IMA Journal of Applied Mathematics (Institute of Mathematics and Its Applications) **76**, 672 (2011).
 - [10] A. Bobylev, The chapman-enskog and grad methods for solving the boltzmann equation, in *Akademiia Nauk SSSR Doklady*, Vol. 262 (1982) pp. 71–75.
 - [11] W. Weiss, Continuous shock structure in extended thermodynamics, Physical Review E **52**, R5760 (1995).
 - [12] J. Hana, C. Ma, Z. Ma, and E. Weinan, Uniformly accurate machine learning-based hydrodynamic models for kinetic equations, Proceedings of the National Academy of Sciences of the United States of America 10.1073/pnas.1909854116 (2019).
 - [13] J. Zhang and W. Ma, Data-driven discovery of governing equations for fluid dynamics based on molecular simulation, Journal of Fluid Mechanics 10.1017/jfm.2020.184 (2020).
 - [14] M. Raissi, P. Perdikaris, and G. E. Karniadakis, Machine learning of linear differential equations using Gaussian processes, Journal of Computational Physics 10.1016/j.jcp.2017.07.050 (2017), arXiv:1701.02440.
 - [15] S. H. Rudy, S. L. Brunton, J. L. Proctor, and J. N. Kutz, Data-driven discovery of partial differential equations, Science Advances 10.1126/sciadv.1602614 (2017), arXiv:1609.06401.
 - [16] H. Schaeffer, Learning partial differential equations via data discovery and sparse optimization, Proceedings of the Royal Society A: Mathematical, Physical and Engineering Sciences 10.1098/rspa.2016.0446 (2017).
 - [17] M. Raissi, P. Perdikaris, and G. E. Karniadakis, Physics-informed neural networks: A deep learning framework for solving forward and inverse problems involving nonlinear partial differential equations, Journal of Computational Physics 10.1016/j.jcp.2018.10.045 (2019).
 - [18] Z. Long, Y. Lu, X. Ma, and B. Dong, PDE-Net: Learning PDEs from data, in *6th International Conference on Learning Representations, ICLR 2018 - Workshop Track Proceedings* (2018).
 - [19] Z. Long, Y. Lu, and B. Dong, PDE-Net 2.0: Learning PDEs from data with a numeric-symbolic hybrid deep network, Journal of Computational Physics **399**, 10.1016/j.jcp.2019.108925 (2019), arXiv:1812.04426.
 - [20] Y. LeCun, Y. Bengio, *et al.*, Convolutional networks for images, speech, and time series, The handbook of brain theory and neural networks **3361**, 1995 (1995).
 - [21] N. Dal Santo, S. Deparis, and L. Pegolotti, Data driven approximation of parametrized PDEs by reduced basis and neural networks, Journal of Computational Physics **416**, 109550 (2020), arXiv:1904.01514.

- [22] A. G. Baydin, B. A. Pearlmutter, A. A. Radul, and J. M. Siskind, Automatic differentiation in machine learning: a survey, *Journal of machine learning research* **18** (2018).
- [23] S. Chapman and T. G. Cowling, *The mathematical theory of non-uniform gases: an account of the kinetic theory of viscosity, thermal conduction and diffusion in gases* (Cambridge university press, 1990).
- [24] R. K. Agarwal, K.-Y. Yun, and R. Balakrishnan, Beyond navier–stokes: Burnett equations for flows in the continuum–transition regime, *Physics of Fluids* **13**, 3061 (2001).
- [25] E. M. Lifshitz and L. P. Pitaevskii, *Statistical physics: theory of the condensed state*, Vol. 9 (Elsevier, 2013) Chap. 88, p. 372.
- [26] L. D. Landau and E. M. Lifshitz, *Course of theoretical physics*, Vol. 5 (Elsevier, 2013) Chap. 112, p. 340.
- [27] V. Michalis, A. Kalarakis, E. Skouras, and V. Burganos, Rarefaction effects on gas viscosity in the knudsen transition regime, *Microfluidics and Nanofluidics* **9**, 847 (2010).
- [28] V. Ghaem-Maghami and A. D. May, Rayleigh-brillouin spectrum of compressed he, ne, and ar. ii. the hydrodynamic region, *Physical Review A* **22**, 698 (1980).
- [29] J. D. Jackson, *Classical electrodynamics* (1999).
- [30] L. D. Landau, *The classical theory of fields*, Vol. 2 (Elsevier, 2013).
- [31] R. Pecora, Doppler shifts in light scattering from pure liquids and polymer solutions, *The Journal of Chemical Physics* **40**, 1604 (1964).
- [32] C. W. Kilmister and C. Cercignani, The Boltzmann Equation and Its Applications, *The Mathematical Gazette* 10.2307/3618229 (1989).
- [33] D. P. Kingma and J. L. Ba, Adam: A method for stochastic optimization, in *3rd International Conference on Learning Representations, ICLR 2015 - Conference Track Proceedings* (2015) arXiv:1412.6980.
- [34] L. Wu and X.-J. Gu, On the accuracy of macroscopic equations for linearized rarefied gas flows, *Advances in Aerodynamics* **2**, 10.1186/s42774-019-0025-4 (2020).

Appendix A: Non-dimensionalization of the governing equation

In system equation

$$\begin{aligned} \frac{\partial \rho}{\partial t} + \frac{\partial v}{\partial x} &= 0 \\ \frac{\partial v}{\partial t} + \frac{\partial T}{\partial x} + \frac{\partial \rho}{\partial x} &= -\text{Kn} \frac{\partial \sigma}{\partial x} \\ \frac{3}{2} \frac{\partial T}{\partial t} + \frac{\partial \rho}{\partial x} &= -\frac{15}{4} \text{Kn} \frac{\partial q}{\partial x}, \end{aligned} \quad (\text{A1})$$

the non-dimensionalization use the reference length scale $\Delta x = \frac{2\pi}{k}$, and the reference time scale follows $\frac{\Delta x}{\Delta t} = \sqrt{\frac{k_B T_0}{m}}$. The non-dimensionalized quantity is represented with bar as $\bar{t} = \frac{t}{\Delta t}$, $\bar{x} = \frac{x}{\Delta x}$, $\bar{v}_x = \frac{\Delta t v_x}{\Delta x}$, $\bar{\rho} = \frac{\rho - \rho_0}{\rho_0}$, $\bar{T} = \frac{T - T_0}{T_0}$, $\bar{\sigma}_{xx} = \frac{m}{\rho_0 k_B T_0} \sigma_{xx}$, $\bar{q}_x = \frac{1}{\rho_0} \left(\frac{m}{k_B T_0} \right)^{3/2} q_x$.

Appendix B: The equivalence between constitutive relation model and scaling laws

This section we will show that the constitutive relation model

$$\begin{aligned} \sigma &= - \sum_{n=1}^{\infty} \left(a_n \frac{\partial^n v}{\partial x^n} + c_n \frac{\partial^n \rho}{\partial x^n} + e_n \frac{\partial^n T}{\partial x^n} \right) \\ q &= - \sum_{n=1}^{\infty} \left(b_n \frac{\partial^n T}{\partial x^n} + d_n \frac{\partial^n \rho}{\partial x^n} + f_n \frac{\partial^n v}{\partial x^n} \right) \end{aligned} \quad (\text{B1})$$

is equivalent to the scaling law in the form

$$\begin{aligned} \sigma(k) &= -ik \frac{4}{3} \frac{\mu(k)}{\mu_0} \tilde{v}_k; \quad \mu(k) \geq 0 \\ q(k) &= -ik \frac{\kappa(k)}{\kappa_0} \tilde{T}_k; \quad \kappa(k) \geq 0. \end{aligned} \quad (\text{B2})$$

As we discussed in the paper, to produce non-negative entropy, stress depends on velocity only, the same as heat flux depending on temperature, since density, velocity, and temperature are statistically independent. Therefore the linear constitutive relations reduce to the form

$$\begin{aligned} \sigma &= - \sum_{n=1}^{\infty} a_n \frac{\partial^n v_x}{\partial x^n} \\ q &= - \sum_{n=1}^{\infty} b_n \frac{\partial^n T}{\partial x^n}, \end{aligned} \quad (\text{B3})$$

under the condition of non-increasing entropy. The non-dimensionalized form of these well defined linear constitutive relations are

$$\begin{aligned} \bar{\sigma}_{xx} &= - \sum_{n=1}^{\infty} \frac{a_n}{\mu \Delta x^{n-1}} \frac{\partial^n \bar{v}_x}{\partial \bar{x}^n} = - \sum_{n=1}^{\infty} \bar{a}_n \frac{\partial^n \bar{v}_x}{\partial \bar{x}^n} \\ \bar{q}_x &= - \sum_{n=1}^q \frac{b_n}{\kappa \Delta x^{n-1}} \frac{\partial^n \bar{T}}{\partial \bar{x}^n} = - \sum_{n=1}^q \bar{b}_n \frac{\partial^n \bar{T}}{\partial \bar{x}^n}, \end{aligned} \quad (\text{B4})$$

in which $\bar{a}_n = \frac{a_n}{\mu \Delta x^{n-1}}$, $\bar{b}_n = \frac{b_n}{\kappa \Delta x^{n-1}}$. Furthermore, analysis the entropy change of the system quantitatively using equation

$$\dot{s} = -\frac{q_j}{T^2} \partial_j T - \frac{\sigma_{ij}}{2T} \left(\frac{\partial v_i}{\partial x_j} + \frac{\partial v_j}{\partial x_i} \right), \quad (\text{B5})$$

tells us that

$$q_j \partial_j T \leq 0; \quad \sigma_{ij} \left(\frac{\partial v_i}{\partial x_j} + \frac{\partial v_j}{\partial x_i} \right) \leq 0. \quad (\text{B6})$$

We require the two term independently satisfy these condition because the temperature and velocity are statistically independent. In our 1D case, more explicitly, we have

$$q_x \partial_x T \leq 0; \quad \sigma_{xx} \partial_x v_x \leq 0 \quad (\text{B7})$$

Especially, if the system is not affected externally, there should not exist a particular scale that entropy decrease. We expect entropy are non-decreasing for each scale. This means for each Fourier modes with wavenumber k we expect

$$\tilde{q}_k(ik\tilde{T}_k)^* \leq 0; \quad \tilde{\sigma}_k(ik\tilde{v}_k)^* \leq 0 \quad (\text{B8})$$

The $*$ indicates complex conjugate. Combine with our linear model B3, after a Fourier transformation on spatial coordinate, we have the condition

$$\begin{aligned} \sum_{n=1}^{\infty} (ik)^{n+1} a_n |\tilde{v}_k|^2 &\leq 0 \\ \sum_{n=1}^{\infty} (ik)^{n+1} b_n |\tilde{T}_k|^2 &\leq 0 \end{aligned} \quad (\text{B9})$$

The previous equation requires that there are no imaginary part on the LHS. Hence only terms with even powers on i remains. Explicitly, we have the constraints

$$\begin{aligned} (k^2 a_1 - k^4 a_3 + k^6 a_5 - k^8 a_7 \dots) |\tilde{v}_k|^2 &\geq 0 \\ (k^2 b_1 - k^4 b_3 + k^6 b_5 - k^8 b_7 \dots) |\tilde{T}_k|^2 &\geq 0 \end{aligned} \quad (\text{B10})$$

The non-dimensionalized version of the constitutive relation therefore becomes

$$\begin{aligned} \partial_{\bar{x}} \bar{\sigma}(\bar{k}) &= (\bar{k}^2 \bar{a}_1 - \bar{k}^4 \bar{a}_3 + \bar{k}^6 \bar{a}_5 \dots) \bar{v}_{\bar{k}} = \bar{k}^2 M(\bar{k}) \bar{v}_{\bar{k}} \\ \partial_{\bar{x}} \bar{q}(\bar{k}) &= (\bar{k}^2 \bar{b}_1 - \bar{k}^4 \bar{b}_3 + \bar{k}^6 \bar{b}_5 \dots) \bar{T}_{\bar{k}} = \bar{k}^2 K(\bar{k}) \bar{T}_{\bar{k}}, \end{aligned} \quad (\text{B11})$$

in which function M, K are the infinite sum of series and should be nonnegative even functions of \bar{k} . We could further deduce the stress and heat flux by removing the spatial derivative:

$$\begin{aligned} \bar{\sigma}(\bar{k}) &= -i\bar{k} M(\bar{k}) \bar{v}_{\bar{k}} \quad M(\bar{k}) \geq 0 \\ \bar{q}(\bar{k}) &= -i\bar{k} K(\bar{k}) \bar{T}_{\bar{k}} \quad K(\bar{k}) \geq 0. \end{aligned} \quad (\text{B12})$$

Functions M, K are closely related to viscosity and heat conduction coefficients. They could be written in the following form

$$\begin{aligned} M(\bar{k}) &= \frac{4}{3} \frac{\mu(\bar{k})}{\mu_0} \\ K(\bar{k}) &= \frac{\kappa(\bar{k})}{\mu_0} \end{aligned} \quad (\text{B13})$$

in which $\mu(\bar{k}), \kappa(\bar{k})$ are scaling laws of viscosity and heat conduction coefficients.

Appendix C: Rayleigh Scattering Background

The Rayleigh scattering has been discovered by Lord Rayleigh back in the nineteenth century. It is the reason for the blue color of the sky in daytime and twilight. As we have mentioned in the method section,

the Rayleigh scattering describes the refraction of electromagnetic waves (EM waves) passing through media with density fluctuation, which leads to refraction index fluctuation[29, 30]. Considering incident wave as plain EM wave with given wavevector \mathbf{k}_i ,

$$\begin{aligned} \mathbf{E}_{inc} &= \boldsymbol{\xi}_0 \exp(i\mathbf{k}_i \cdot \mathbf{r} - i\omega_i t) \\ |\mathbf{k}_i| &= \frac{\sqrt{\epsilon_0} \omega_i}{c} \end{aligned} \quad (\text{C1})$$

With $\boldsymbol{\xi}_0$ be the polarization vector, \mathbf{k}_i the incident wave vector, ω_i the incident wave frequency, and ϵ_0 the dielectric constant of gas. The refraction index fluctuation is proportional to the dielectric constant of the gas $\epsilon(\rho)$, hence related to the density fluctuation to the density fluctuation as the following perturbation relation

$$\epsilon = \epsilon_0 + \partial_{\rho} \epsilon(\rho_0) \delta \rho + \dots \quad (\text{C2})$$

where the ρ_0 is the density of gas and $\delta \rho$ is the fluctuation of the gas density. The scattered spectra I is defined by the autocorrelation function of scattered electric field \mathbf{E}_1 .

$$\mathbf{I}(\omega_f) = \frac{1}{2\pi} \int \langle \mathbf{E}_1(t') \cdot \mathbf{E}_1(t' + t) \rangle \exp(-i\omega_f t) dt \quad (\text{C3})$$

In which the $\langle Q \rangle$ means the ensemble average of the quantity Q . The scattered spectra I could be calculated by perturbation method is as follows [31]

$$\begin{aligned} \mathbf{I}(\omega_f) &= \frac{N \omega_i^4 |\boldsymbol{\xi}_0|^2 \sin^2(\psi)}{32\pi^3 c^4 r^2} [\partial_{\rho} \epsilon(\rho_0)]^2 \\ &\int dt \int d\mathbf{r}^3 e^{-i(\omega_f - \omega_i)t} e^{-i(\mathbf{k}_i - \mathbf{k}_f) \cdot \mathbf{r}} (G(\mathbf{r}, t) - \rho_0) \\ G(\mathbf{r}, t) &= \frac{1}{N} \left\langle \int d\mathbf{r}'^3 \rho(\mathbf{r}' - \mathbf{r}, 0) \rho(\mathbf{r}', t) \right\rangle \end{aligned} \quad (\text{C4})$$

in which the G is the so-called density correlation function. N represents the total number of gas molecules we are considering in our integration domain, \mathbf{k}_f the scattered wave vector, ω_f the scattered wave frequency, c is the speed of light in vacuum and r is the distance between the scattering gas medium and observer. It is easy to derive that the term inside the integral of first equation in C4 is proportional to the density fluctuation spectra $\langle \rho^2 \rangle(\mathbf{k}_i - \mathbf{k}_f, \omega_i - \omega_f)$ for given $\mathbf{k}_i, \mathbf{k}_f$. The density fluctuation spectra is defined as, for density function $\rho(t)$, that

$$\begin{aligned} \langle \rho^2 \rangle(\omega, \mathbf{k}) &= \frac{1}{2\pi} \int \langle \rho^2 \rangle(t, \mathbf{x}) e^{-i\omega t} e^{-i\mathbf{k} \cdot \mathbf{x}} dt d\mathbf{x} \\ \langle \rho^2 \rangle(t, \mathbf{x}) &= \langle \rho(t_0, \mathbf{x}_0) \rho(t_0 + t, \mathbf{x}_0 + \mathbf{x}) \rangle \end{aligned} \quad (\text{C5})$$

In summary, the key of calculating the Rayleigh scattering spectra is to calculate the density fluctuation spectra.

Appendix D: Calculating the density fluctuation spectra

Substitute the our model into (A1), for monatomic gas with the heat conduction coefficient $\kappa = \frac{15k_B}{4m}\mu$, we have the non-dimensionalized system equation to be

$$\begin{aligned} \partial_{\bar{t}}\delta\bar{\rho} + \partial_{\bar{x}}\bar{v}_x &= 0 \\ \partial_{\bar{t}}\bar{v}_x + \partial_{\bar{x}}\delta\bar{T} + \partial_{\bar{x}}\delta\bar{\rho} &= \text{Kn} \sum_{n=1}^{\infty} \bar{a}_n \partial_{\bar{x}}^{n+1} \bar{v}_x \\ \frac{3}{2}\partial_{\bar{t}}\delta\bar{T} + \partial_{\bar{x}}\bar{v}_x &= \frac{15}{4}\text{Kn} \sum_{n=1}^{\infty} \bar{b}_n \partial_{\bar{x}}^{n+1} \bar{T} \end{aligned} \quad (\text{D1})$$

Multiply $\rho(0,0)$ and take ensemble average, we could obtain a system on correlation functions such as $\langle\rho^2\rangle(t,x)$, $\langle\rho v_x\rangle(t,x)$, etc. These function are well defined since we are considering homogeneous gas, hence the fluctuations are stationary.

Before we preceed, we define the one sided Fourier transform on time coordinate:

$$x_{\omega}^{(+)} = \frac{1}{\sqrt{2\pi}} \int_0^{\infty} x(t) e^{-i\omega t} dt. \quad (\text{D2})$$

And in this section we omit the bar that indicating non-dimensionalized variables.

Doing a Fourier transform on space coordinate, and one sided Fourier transformation on time coordinate, the macroscopic equation becomes

$$\begin{aligned} i\omega \langle\rho^2\rangle_{\omega,k}^{+} + ik \langle\rho v_x\rangle_{\omega,k}^{+} &= \frac{1}{\sqrt{2\pi}} \langle\rho^2\rangle_k \\ i\omega \langle\rho v_x\rangle_{\omega,k}^{+} + ik \langle\rho T\rangle_{\omega,k}^{+} + ik \langle\rho^2\rangle_{\omega,k}^{+} &= \\ -k^2 \text{Kn} M(Kn) \langle\rho v_x\rangle_{\omega,k}^{+} & \\ -\frac{3}{2}i\omega \langle\rho T\rangle_{\omega,k}^{+} + ik \langle\rho v_x\rangle_{\omega,k}^{+} &= -\frac{15}{4}k^2 \text{Kn} K(Kn) \langle\rho T\rangle_{\omega,k}^{+} \end{aligned} \quad (\text{D3})$$

$$\langle\rho^2\rangle_{\omega,k}^{+} = -\frac{ikN_{eff}m(-2k^4 A(Kn)B(Kn) - 3ik^2\omega A(Kn) - 2ik^2\omega B(Kn) - 2k^2 + 3\omega^2)}{(2\pi)^2\rho_0(-2k^4\omega A(Kn)B(Kn) - 3ik^2\omega^2 A(Kn) + 2ik^4 B(Kn) - 2ik^2\omega^2 B(Kn) - 5k^2\omega + 3\omega^3)} \quad (\text{D7})$$

The NS equation also lies in the framework of linear constitutive relation model. We just need to set the following relation

$$M(Kn) = \frac{4}{3}, \quad (\text{D8})$$

combined with equation in the paper

$$\kappa(\text{Kn}) = \frac{5k_B}{2m} \frac{\mu(\text{Kn})}{\text{Pr}}, \quad \text{Pr} = \frac{2}{3}. \quad (\text{D9})$$

The spectra hence follows the same form as in equation D7.

The term $\langle\rho^2\rangle_k$ on the left hand side of the first equation in D3 comes from integration by part. This is the spatial density fluctuation spectra which is a constant, since there are no spatial correlation between different location at macroscopic level. The term $\langle\rho^2\rangle_k$ could be calculated from fluctuation theory [26]

$$\langle\rho^2\rangle_k = \frac{mN_{eff}k}{(2\pi)^{3/2}\rho_0} \quad (\text{D4})$$

Where the m is the molecule mass, and the N_{eff} is the effective number of molecules per particle used in the DSMC simulation, to take the Monte Carlo fluctuation into account. The integration by part will also give terms such as $\langle\rho v\rangle_k$ and $\langle\rho T\rangle_k$. However, it is known that they vanish according to fluctuation theory.

The density fluctuation spectra could be obtained from the spectra $\langle\tilde{\rho}^2\rangle_{\omega,k}^{+}$ which takes one sided Fourier transform on time coordinate and Fourier transform on spatial coordinate. The following relation could be used to obtain the density fluctuation spectra:

$$\langle\rho^2\rangle_{\omega} = \langle\rho^2\rangle_{\omega}^{(+)} + \langle\rho^2\rangle_{\omega}^{(+)*} \quad (\text{D5})$$

Substitute the linear constitutive relation model into the system equation, we have the system D3, combined with the initial condition D4. The term $\langle\rho^2\rangle_{\omega,k}^{+}$ could be solved from the system, with the notation

$$\begin{aligned} A(Kn) &= KnM(Kn) \\ B(Kn) &= \frac{15}{4}KnK(Kn). \end{aligned} \quad (\text{D6})$$

The solution for $\langle\rho^2\rangle_{\omega,k}^{+}$ is

As for the Grad 13 method, two addition equation on the stress and heat flux appears. as is

$$\begin{aligned} \partial_t\sigma + \frac{4}{3}\partial_x v_x + \frac{8}{15}\partial_x q &= -\frac{\sigma}{Kn} \\ \partial_t q + \partial_x\sigma + \frac{5}{2}\partial_x T &= -\frac{2}{3}\frac{q}{Kn} \end{aligned} \quad (\text{D10})$$

Again, Multiply $\rho(0,0)$ and take ensemble average, we could obtain another system on correlation functions. Doing a one sided Fourier transformation on time and Fourier transformation on space coordinates, we have

$$\begin{aligned}
i\omega \langle \rho^2 \rangle_{\omega,k}^+ + ik \langle \rho v_x \rangle_{\omega,k}^+ &= \frac{mN_{eff}k}{(2\pi)^2\rho_0} \\
i\omega \langle \rho v_x \rangle_{\omega,k}^+ + ik \langle \rho T \rangle_{\omega,k}^+ + ik \langle \rho^2 \rangle_{\omega,k}^+ + ik \langle \rho \sigma \rangle_{\omega,k}^+ &= 0 \\
\frac{3}{2}i\omega \langle \rho T \rangle_{\omega,k}^+ + ik \langle \rho v_x \rangle_{\omega,k}^+ + ik \langle \rho q \rangle_{\omega,k}^+ &= 0 \\
i\omega \langle \rho \sigma \rangle_{\omega,k}^+ + \frac{4}{3}ik \langle \rho v_x \rangle_{\omega,k}^+ + \frac{8}{15}ik \langle \rho q \rangle_{\omega,k}^+ &= -\frac{\langle \rho \sigma \rangle_{\omega,k}^+}{Kn} \\
i\omega \langle \rho q \rangle_{\omega,k}^+ + ik \langle \rho \sigma \rangle_{\omega,k}^+ + \frac{5}{2}ik \langle \rho T \rangle_{\omega,k}^+ &= -\frac{2}{3} \frac{\langle \rho q \rangle_{\omega,k}^+}{Kn}
\end{aligned} \tag{D11}$$

The spectra is hence calculated in the same way as NS

equation and linear constitutional relation model. The result is

$$\langle \delta \rho^2 \rangle_{\omega,k,Grad13}^+ = \frac{mN_{eff}k (-36ik^4Kn^2 + 189ik^2Kn^2\omega^2 + 165k^2Kn\omega - 20ik^2 - 45iKn^2\omega^4 - 75Kn\omega^3 + 30i\omega^2)}{(2\pi)^2\rho_0 (135k^4Kn^2\omega - 75ik^4Kn - 234k^2Kn^2\omega^3 + 240ik^2Kn\omega^2 + 50k^2\omega + 45Kn^2\omega^5 - 75iKn\omega^4 - 30\omega^3)} \tag{D12}$$

As for the velocity fluctuation spectra, the LHS of D3 need to be modified, since this time we product $v_x(0,0)$

instead of $\rho(0,0)$ before taking the ensemble average. This time we have

$$\begin{aligned}
i\omega \langle \rho v_x \rangle_{\omega,k}^+ + ik \langle v_x^2 \rangle_{\omega,k}^+ &= 0 \\
i\omega \langle v_x^2 \rangle_{\omega,k}^+ + ik \langle v_x T \rangle_{\omega,k}^+ + ik \langle \rho v_x \rangle_{\omega,k}^+ &= -k^2 A(Kn) \langle \rho v_x \rangle_{\omega,k}^+ + \frac{N_{eff}mk}{(2\pi)^2\rho_0} \\
\frac{3}{2}i\omega \langle v_x T \rangle_{\omega,k}^+ + ik \langle v_x^2 \rangle_{\omega,k}^+ &= -k^2 B(Kn) \langle v_x T \rangle_{\omega,k}^+
\end{aligned} \tag{D13}$$

$$\langle \delta v_x^2 \rangle_{\omega,k}^+ = -\frac{iN_{eff}m\omega k (3\omega - 2ik^2 B(Kn))}{(2\pi)^2\rho_0 (-2k^4\omega A(Kn)B(Kn) - 3ik^2\omega^2 A(Kn) + 2ik^4 B(Kn) - 2ik^2\omega^2 B(Kn) - 5k^2\omega + 3\omega^3)} \tag{D14}$$

Appendix E: DSMC calculation Details

We use the DSMC0F program by A.Bird [4] to simulate the fluctuation of 1D homogeneous gas. The computing details are shown in following Table I using SI units. A snap shot will be stored for every 5 time steps. Then the macroscopic quantities for each cell are calculated by averaging corresponding quantites of particles in each cell. The density fluctuation spectra used to train the neural network is ensemble average from 27 independent DSMC run.

Appendix F: Neural Network Training Details

The density fluctuation spectra is of the form $\langle \rho^2 \rangle(k, \omega)$, with k corresponds to the wave number of our interested density fluctuation wave, which directly determines the Knudsen number, and ω be the frequency of the corresponding wave. Given k , the spectra $\langle \rho^2 \rangle_k(\omega)$ is a function of the angular frequency ω with spectra structure caused by collective behavior of gas molecules. Duirng training process of linear constitutive relation model, 200 k is draw from a uniform distribution on the interval $\left[0, \frac{\pi\rho_0}{2\mu} \sqrt{\frac{k_B T_0}{m}}\right]$. for a given k , we do a

TABLE I. The coefficients and configuration used in DSMC0F program.

Domain Length	4.8	Collision Model	VHS ^a
Power law ^b	0.5	Diameter ^c	3.5×10^{-10}
Num of Cell	1281	Mean Free Path	1.8×10^{-2}
Simulation Particle	128100	Mean Free Time	4×10^{-5}
Density	5×10^{-6}	Temperature	300
Molecule Mass	5×10^{-26}	Sound Speed	371.56
Heat Conduction	0.0214	Viscosity	2.07×10^{-5}
Δt	4×10^{-6}	Δx	3.7×10^{-3}
Subcell ^d	8		

^a Variable hard sphere model

^b The viscosity-temperature power law used in variable hard sphere model

^c The reference molecule diameter

^d The number of subcell per cell used in particle collision process

Monte Carlo sample using acceptance-rejection method, 200 draw of ω from the range $[-3ck, 3ck]$ with probabil-

ity proportional to $\langle \rho^2 \rangle_k(\omega)$ calculated using DSMC. c is the speed of sound. Finally, the training data set consists of total 40000 $(k, \omega, \langle \rho^2 \rangle)$ tuple. In the same way, we sample another 400 tuple as validation set.

The function M is modeled as a fully connected neural network as shown in the paper. The weights to be trained is $\mathbf{W}_{1,2}$, notice that in our linear layer, there is no bias as usual. This is because we need a function to satisfy constraints as discussed in the paper. The weights are initialized using uniform initialization by default in Pytorch. We then compare the mean square difference between spectra $\langle \rho^2 \rangle_k(\omega)$ computed using DSMC with the spectra predicted by linear constitutive relation model. The optimizer we use is the Adam optimizer with learning rate $\alpha = 0.005$, Beta parameter $\beta_1 = 0.9$ and $\beta_2 = 0.999$, and the parameter $\epsilon = 10^{-8}$. For each training epoch, the batch size for each step is 64. The training process stops if the loss obtained on validation set increases. Since we are doing 1D function fitting using thousands of data, over-fitting is negligible, this is also tested by the velocity spectra predicted by our model.